

## 3D FIB/SEM study of Ni<sub>4</sub>Ti<sub>3</sub> precipitates in Ni-Ti alloys with different thermal-mechanical histories

S. Cao<sup>1a</sup>, M. Nishida<sup>2</sup>, Ch. Somsen<sup>3</sup>, G. Eggeler<sup>3</sup>, D. Schryvers<sup>1</sup>

<sup>1</sup>EMAT, University of Antwerp, Groenenborgerlaan 171, B-2020, Antwerp, Belgium

<sup>2</sup>Department of Engineering Sciences for Electronics and Materials, Kyushu University, Kasuga 816-8580, Japan

<sup>3</sup>Institute for Materials, Ruhr University Bochum, D-44780 Bochum, Germany

**Abstract.** The three-dimensional size, morphology and distribution of Ni<sub>4</sub>Ti<sub>3</sub> precipitates growing in binary Ni-rich Ni-Ti alloys have been investigated via a slice & view procedure in a Dual-Beam FIB/SEM system, in order to better understand their influence on the B2 to B19' martensitic transformation. In the present work, both a stress-free Ni<sub>50.8</sub>Ti<sub>49.2</sub> alloy with all four variants of precipitates and a compressed Ni<sub>51</sub>Ti<sub>49</sub> alloy with aligned precipitates in one family were studied. The Ni<sub>4</sub>Ti<sub>3</sub> precipitates reach a volume fraction of 9.6% in the reconstructed region of the stress-free alloy and 4.3% in the compressed one. In both cases, the mean volume, specific surface area, sphericity and aspect ratio of the precipitates are calculated and the Pair Distribution Functions of the precipitates are obtained. It is shown that most precipitates in the stress-free sample grow larger and have a more lenticular shape, while those in the compressed sample are more cylindrical. Deviations from these ideal shapes reveal internal steps in the stress-free sample and lamellae formation in the compressed one.

### 1. Introduction

Binary Ni-rich Ni-Ti alloys have been widely studied and applied for their unique properties in shape memory and superelasticity [1, 2]. The morphology and microstructure of Ni<sub>4</sub>Ti<sub>3</sub> precipitates in the austenite matrix of these alloys has caused increasing interest because of their significant influence on the B2-B19' martensitic transformation of the matrix [1]. The Ni<sub>4</sub>Ti<sub>3</sub> precipitates normally have a lenticular morphology (micro-scale in length, nano-scale in width) with a central plane (habit plane) which is parallel to the {111} planes of the B2 matrix. There are 8 variants of Ni<sub>4</sub>Ti<sub>3</sub> precipitates in total, but since two ordered variants share one habit plane, only four different orientations will be observed in conventional Scanning Electron Microscopy (SEM). The Ni<sub>4</sub>Ti<sub>3</sub> precipitates have a rhombohedral atomic structure with  $a=0.670\text{nm}$ ,  $\alpha=113.9^\circ$  [3] (or  $a=b=1.124\text{nm}$ ,  $c=0.5077\text{nm}$  in the hexagonal description [4]), which has recently been refined by dedicated electron diffraction to a space group R-3 [5] and neutron diffraction [6], while the lattice parameter of the B2 structure of the matrix equals 0.301 nm [4].

Moreover, the actual size and distribution of the Ni<sub>4</sub>Ti<sub>3</sub> precipitates depends strongly on the thermo-mechanical history of the material. Short and intermediate term stress free aging can lead to heterogeneous microstructures with precipitates concentrating around grain boundaries, splitting the transformation into several steps upon cooling [7,8,9] while compressing or elongating the sample during heating can introduce preferential growth of a single variant [10,11,12]. Also, the volume fraction of precipitates will influence the overall as well as local composition of the matrix, having a strong effect on the martensite transformation temperatures [13,14]. In other words, the study of the three-dimensional distribution of these precipitates is of great importance for any application of Ni-Ti SMA.

In the present study, a Slice-and-View procedure in a Dual-Beam FIB/SEM system is applied to investigate both a stress-free Ni<sub>50.8</sub>Ti<sub>49.2</sub> alloy with all four variants of precipitates and a single crystal Ni<sub>51</sub>Ti<sub>49</sub> alloy after <111> compression ageing with precipitates aligned in one family, in order to reveal the different characteristics of the 3D configuration of precipitates in the alloys treated under different conditions. The parameters investigated for a set of precipitates include volume fraction, specific surface area and aspect ratio, while the distribution of precipitates is described by a pair distribution function.

<sup>a</sup> e-mail: [Shanshan.Cao@ua.ac.be](mailto:Shanshan.Cao@ua.ac.be)

## 2. Experiment

### 2.1 Sample preparation

For the stress-free alloy, a Ti-50.8at.%Ni alloy is solution treated in a vacuum sealed quartz tube at 1273K for 3.6ks, followed by water quenching. Afterwards, the alloy is aged at 773k for 3.6ks in order to generate heterogeneous microstructures with small  $\text{Ni}_4\text{Ti}_3$  precipitates with a central plane diameter of around 80-200nm concentrated around grain boundaries and larger precipitates with a central plane diameter of around  $1\mu\text{m}$  scattered in the grain interior (Figure 1). A foil with a thickness around 1mm is well polished for the Slice-and-View approach in the Dual Beam. In the present study, a grain interior region with relatively large but few precipitates in this stress-free sample is selected for the investigation.

On the other hand, for the compressed alloy, a single crystal of millimeter size of  $\text{Ni}_{51}\text{Ti}_{49}$  is produced via the Bridgman technique [10]. After a homogenization treatment at 1273K for 12h followed by water quenching, a stress-assisted  $\langle 111 \rangle$  compression ageing at 823K/50MP for 36ks is performed on the cylinder sample to introduce parallel  $\text{Ni}_4\text{Ti}_3$  precipitates with a central plane diameter of around  $1\mu\text{m}$  and perpendicular to the  $[111]_{\text{B}_2}$  compression direction. A sample with a thickness of around 0.5mm is sliced from the top of the cylinder along the  $(111)_{\text{B}_2}$  plane and polished for the Slice-and-View approach in the Dual Beam.

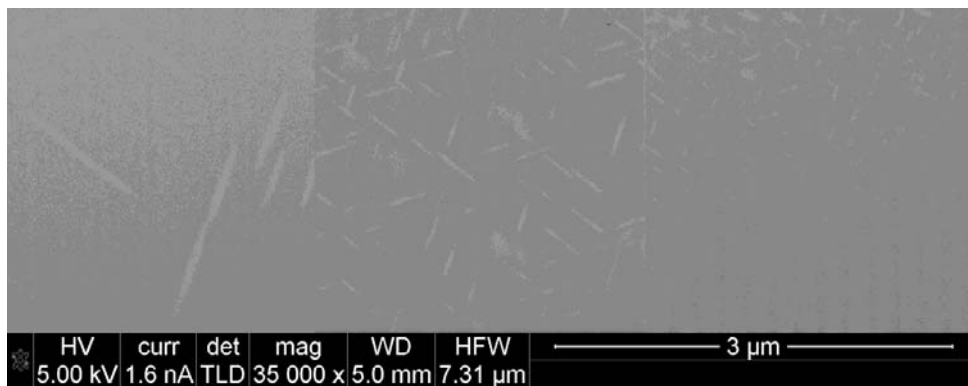


**Fig. 1.** Evolution of the  $\text{Ni}_4\text{Ti}_3$  precipitates in size and distribution from grain interior (left) to grain boundary in the stress-free sample.

### 2.2 Image acquisition and processing

A Dual-Beam FIB/SEM xT Nova Nanolab 200 is used in the present work to obtain the 2D cross-section images of the Ni-Ti samples. The main steps of the image acquisition and treatment relate to the weak contrast of the precipitates due to their similar composition and structure as the surrounding matrix [15]. Sequences of around 100 2D cross-section images with intervals of 25 nm are obtained for both alloys, from which the 3D data sets result after substantial image processing. Two examples of the SEM cross-section images from these two alloys are shown in Figure 2, as obtained with the Through Lens Detector (TLD).

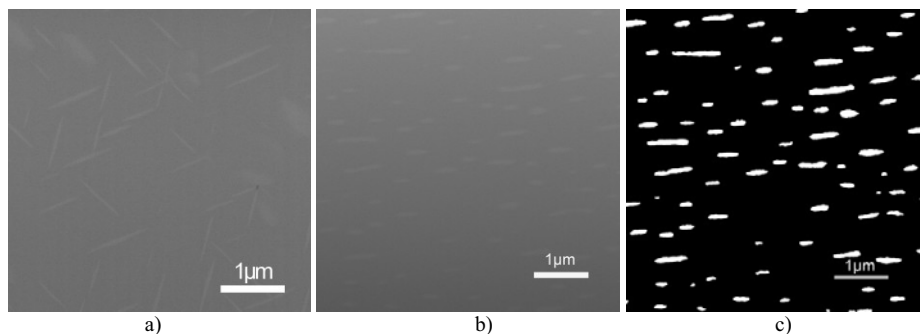


**Fig. 2.** Two examples of the 2D cross-section SEM images from a) grain interior of the stress-free alloy and b) compressed alloy. C) shows a binary image after segmentation.

The principle of 3D reconstruction from 2D cross-section data is well known [15]. After image alignment, resizing and selection of a region of interest, a 2D image sequence with a corrected dimension of

$4.75 \times 4.75 \mu\text{m}^2$  is obtained for the stress-free alloy, while a sequence with a corrected dimension of  $5.55 \times 5.53 \mu\text{m}^2$  is obtained for the compressed alloy. To ensure the precision of the 3D reconstruction, especially for the ensuing quantitative analysis, some image processing is necessary to improve the image quality. In MatLab<sup>®</sup>, a combination of image filters (*wiener2*, *imadjust* and *imsubtract*) are applied on the entire sequence of 2D images in order to decrease noise, improve image contrast and remove the background.

For the stress-free alloy, the optimized image sequence is segmented in Amira<sup>®</sup> with the *label field* function to differentiate different variants of  $\text{Ni}_4\text{Ti}_3$  precipitates from each other and the matrix. While for the compressed alloy, due to the single variant of  $\text{Ni}_4\text{Ti}_3$  precipitates, some more image filters (*graythresh* and *im2bw*) are applied to convert the improved images into binary ones, following the segmentation in Amira<sup>®</sup> with the *labelvoxel* function to differentiate all the  $\text{Ni}_4\text{Ti}_3$  precipitates from the matrix. An example is seen in Figure 2c. Afterwards, the 3D reconstructions with a size of  $4.75 \times 4.75 \times 4.775 \mu\text{m}^3$  for the stress-free alloy and  $5.55 \times 5.53 \times 2.53 \mu\text{m}^3$  for the compressed alloy can be achieved through the *surfacegen* function, as shown in Figure 3a and d. Further qualitative and quantitative analyses on both Ni-Ti alloys are achieved based on these reconstructions.

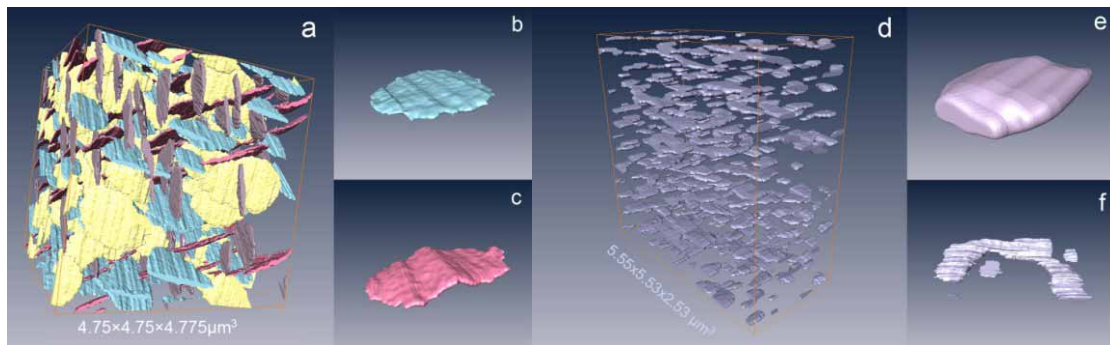


**Fig. 3.** 3D reconstructions of the (a-c) stress-free and (d-f)  $\langle 111 \rangle$  compressed Ni-Ti alloy clearly showing the 4 crossing families in the former and the single family in the latter case.

### 3. Results and discussion

As is clear from Figure 3a, in the interior of the stress-free alloy, the four variants of  $\text{Ni}_4\text{Ti}_3$  precipitates often cross with one another. From the individual example in Figure 3b the typical lenticular shape is seen although several precipitates reveal a less regular morphology with internal steps as in Figure 3c. In the compressed alloy individual precipitates with a close to flat cylindrical morphology can be singled out, as in Figure 3e, i.e. the shape is more disc-like and missing the edge tapering of the lenticular shape in stress-free annealed alloys [15]. However, again in the compressed case some precipitates are seen to be contiguous and to yield lamellae with an irregular morphology, as shown in Figure 3f.

The volume ( $V_p$ ), surface area ( $SA$ ), maximum Feret diameter ( $FD_{max}$ ), minimum Feret diameter ( $FD_{min}$ ) and aspect ratio ( $AR$ ) of each  $\text{Ni}_4\text{Ti}_3$  precipitate in both alloys can directly be obtained via quantitative analysis based on pixel measurements. The  $AR$  is defined as the largest diameter divided by the smallest diameter in its orthogonal plane, while the  $FD_{max}$  and  $FD_{min}$  are considered as the respective clipper estimations of the disc diameter and thickness of the precipitates [16,17]. It should be noted that since the pixel based measurement is discrete,  $V_p$  and  $SA$  can only be estimated by calculating the volume and area in pixels, which implies a decrease in precision. In total, 525 precipitates were found in the stress-free sample and 343 in the compressed one, yielding densities of  $4.9$  and  $4.4 \mu\text{m}^{-3}$ , respectively. With these measured  $V_p$  and  $SA$ , the specific surface area ( $SSA$ ) for each precipitate can be calculated as:

$$SSA = \frac{SA}{V_p} \quad (1)$$

Besides  $AR$  and  $SSA$ , sphericity ( $\psi$ ) is another specific parameter of morphology characterization. It is a measure of how spherical an object is, which implies the compactness of morphology. Defined by Wadell [18], the sphericity of a precipitate is the ratio of the surface area of a sphere with the same volume as the given precipitate to the surface area of the precipitate:

$$\psi = \frac{\pi^{\frac{1}{3}} (6V_p)^{\frac{2}{3}}}{SA} \quad (2)$$

The volume fraction ( $f_v$ ) of all  $\text{Ni}_4\text{Ti}_3$  precipitates in the matrix can further be obtained from:

$$f_v = \frac{\sum_{i=1}^n V_{pi}}{V_{total}} \quad (3)$$

where  $V_{total}$  is the total volume of the reconstructed bulk. All these size and morphology results are presented for both samples in Tables 1 and 2. Here it should be noted that in the present study, precipitates cut by the edge of the reconstruction boxes have also been counted in both cases. This implies an underestimation of the mean  $V_p$ ,  $SA$ ,  $FD_{max}$  and  $AR$ , and an overestimation of the mean  $SSA$  and  $\Psi$ , whereas the volume fraction  $f_v$  remains unaffected. However, comparing between both systems is still possible and apparently, the precipitates in the grain interior of the stress-free sample have a higher volume fraction than those in the compressed sample, which is consistent with the TTT diagram at which the time/temperature point for the compressed sample is close to a transition curve above which  $Ni_3Ti_2$  precipitates will be formed at the expense of the  $Ni_4Ti_3$  ones, whereas the stress-free point is located in the centre of the  $Ni_4Ti_3$  stability region.

The distributions of  $V_p$ ,  $SSA$  and  $AR$  of the 3D data of the precipitates are shown in Figures 4-6, clearly revealing the expected lognormal distributions for these types of measures of precipitates. In the grain interior of the stress-free alloy, more than 67% of the precipitates have a  $V_p$  in the region between  $0.00130\mu m^3$  and  $0.0545\mu m^3$ , an  $SSA$  in the region between  $39.62\mu m^{-1}$  and  $90.34\mu m^{-1}$ , and an  $AR$  in the region between 5.44 and 11.07. On the other hand, in the compressed alloy, more than 67% of the precipitates have a  $V_p$  in the region between  $0.00132\mu m^3$  and  $0.0186\mu m^3$ , an  $SSA$  in the region between  $34.58\mu m^{-1}$  and  $66.43\mu m^{-1}$ , and an  $AR$  in the region between 4.11 and 8.76. It can thus be concluded that the compressed alloy contains precipitates with smaller size, which is consistent with the observations in 2D images. Also, the distribution of sizes as seen in Figure 4 shows a narrower region for the compressed sample, however, it doesn't show a strong peak as in the grain interior of the stress-free alloy. Again, the overall size difference can be linked to the position of the time/temperature point in the TTT diagram, also because the density of precipitates in both systems is very similar. The difference in distribution shape can possibly be connected with the freedom of growth in 1 or 4 directions.

The higher  $AR$  of the precipitates in the grain interior of the stress-free alloy shows they appear more flat in shape than those in the compressed alloy, which might seem strange. At the same time the larger  $SSA$  and lower  $\Psi$  suggest a more complicated shape for the stress-free precipitates. The latter indicates the  $Ni_4Ti_3$  precipitates grow more freely during ageing without pressure, which is not surprising. On the other hand, by comparing the  $FD_{max}$  and  $FD_{min}$  of both types of precipitates, it is clear that  $FD_{min}$  (thickness) only differs by about 10%, while  $FD_{max}$  (diameter of the central plane) changes by about 30%, which implies that the difference in  $AR$  is mainly due to the diameter. The latter can possibly be explained by the space for free growth of the precipitates along their central plane in the stress-free sample.

Based on the mass centers of the  $Ni_4Ti_3$  precipitates, the radial pair distribution function (PDF) is calculated. As seen from Figure 7, for the compressed alloy a first strong peak is found at  $0.56\mu m$  in the radial PDF, indicating the nearest neighbor distance, followed by a second and a third peak at respectively  $0.77\mu m$  and  $1.24\mu m$ . In the grain interior of the stress-free alloy a first strong peak shows up at  $0.44\mu m$  with an extra peak at  $0.26\mu m$  due to intersecting precipitates. A more extended study has shown that the first peak in the compressed sample corresponds to the interparticle distance of  $0.54\mu m$  in the compressed direction even revealing small pockets of channelling [19]. This thus confirms that the precipitates in the compressed alloy not only have smaller sizes, but are also distributed with a lower density.

**Table 1.** Value of the volume fraction and geometric mean values of the size parameters ( $V_p$ ,  $SA$ ) of the  $Ni_4Ti_3$  precipitates in different alloys, including standard deviations

	No. prec.	$f_v$ (%)	$\overline{V_p}$ ( $\mu m^3$ )	$\overline{SA}$ ( $\mu m^2$ )
Stress-Free	525	9.6	0.00842*/6.473	0.50*/4.39
Compressed	343	4.3	0.00495*/3.760	0.24*/2.82

**Table 2.** Geometric mean values of the morphology parameters ( $\Psi$ ,  $SSA$ ,  $FD_{max}$ ,  $FD_{min}$  and  $AR$ ) of the  $Ni_4Ti_3$  precipitates in different alloys, including standard deviations

	$\Psi$	$\overline{SSA}$ ( $\mu m^{-1}$ )	$\overline{FD_{max}}$ ( $\mu m$ )	$\overline{FD_{min}}$ ( $\mu m$ )	$\overline{AR}$
Stress-Free	0.39 */1.30	59.83 */1.51	0.739 */1.957	0.096 */1.686	7.69 */1.44
Compressed	0.59 */1.22	47.93 */1.39	0.514 */1.829	0.085 */1.479	6.00 */1.46

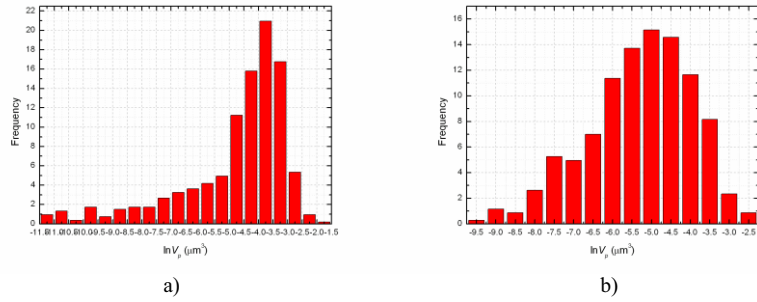


**Fig. 4.** Volume distribution of the precipitates in the (a) stress-free and (b) compressed Ni-Ti alloy using a log measure in the abscissa.

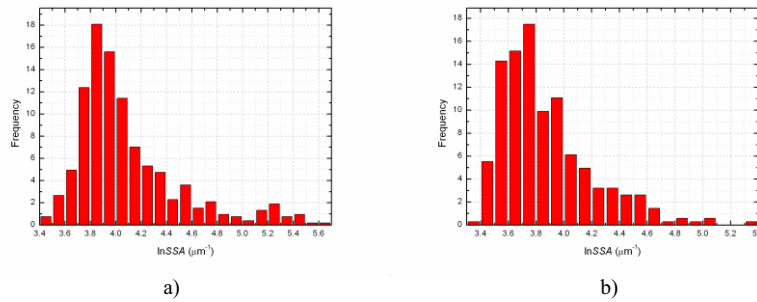


**Fig. 5.** Specific Surface Area distribution of the precipitates in the (a) stress-free and (b) compressed Ni-Ti alloy using a log measure in the abscissa.

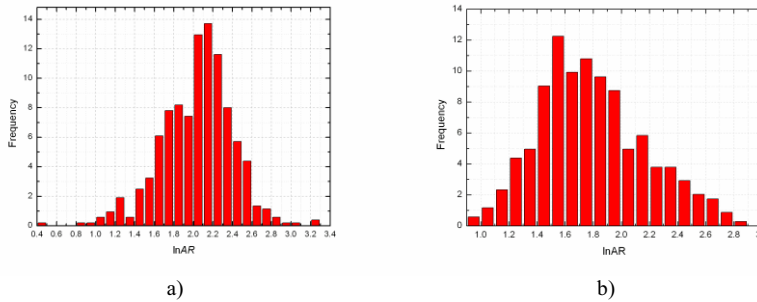


**Fig. 6.** Aspect Ratio distribution of the precipitates in the (a) stress-free and (b) compressed Ni-Ti alloy using a log measure in the abscissa.

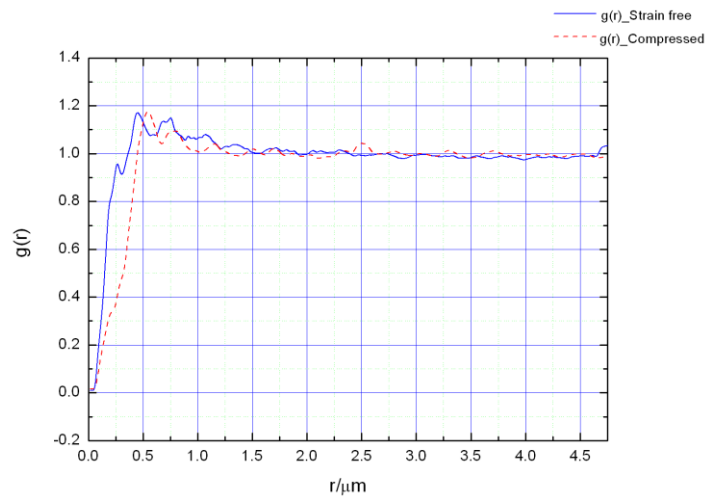


**Fig. 7.** Pair distribution function (PDF) of the precipitate mass centers in the stress-free (full blue) and compressed (dashed red) Ni-Ti alloy.

## 4. Conclusion

In the present study, the 3D size, morphology and distribution of Ni<sub>4</sub>Ti<sub>3</sub> precipitates in both a stress-free Ni<sub>50.8</sub>Ti<sub>49.2</sub> alloy with heterogeneous microstructures and a single crystal Ni<sub>51</sub>Ti<sub>49</sub> alloy after <111> compression are studied via a Slice-and-View procedure in a Dual-Beam FIB/SEM system. The lenticular-shaped Ni<sub>4</sub>Ti<sub>3</sub> precipitates in the grain interior of the stress-free alloy have a higher volume fraction, larger size, are flatter and have a more complicated shape and a higher density than the more cylindrical precipitates of the compressed sample. These difference introduced by the thermo-mechanical histories of the alloys are all revealed in the 3D reconstruction.

## Acknowledgement

The present work was performed in the framework of MULTIMAT “Multi-scale modeling and characterization for phase transformations in advanced materials”, a Marie Curie Research Training Network (MRTN-CT-2004-505226) of the EU. Support was also provided by the FWO project G.0576.09N “Three-dimensional characterization of precipitates in Ni-Ti shape memory alloys by slice-and-view in a FIB-SEM dual-beam microscope”. S. Cao also likes to thank W. Van den Broek for useful suggestions concerning the image processing and M. Croitoru for support with the PDF calculations.

## References

- [1] K. Otsuka and X. Ren, *Prog. Mater. Sci.* **50**, 511 (2005)
- [2] K. Otsuka and C. M. Wayma, *Shape memory materials* (Cambridge University Press, Cambridge, UK, 1998) p. 49
- [3] T. Tadaki, Y. Nakata, K. Shimizu, K. Otsuka, *Trans. Jpn. Inst. Met* **27**, 731 (1986)
- [4] W. Tirry and D. Schryvers, *Acta Mater.* **53**, 1041 (2005)
- [5] W. Tirry, D. Schryvers, K. Jorissen and D. Lamoen, *Acta Crystallogr. B* **62**, 966 (2006)
- [6] J. Khalil-Allafi, W.W. Schmahl, M. Wagner, H. Sitepu, D.M. Toebbens and G. Eggeler, *Mater. Sci. Eng. A* **378**, 161 (2004)
- [7] J. Khalil-Allafi, A. Dlouhy, G. Eggeler, *Acta Mater.* **50**, 4255 (2002)
- [8] G. Fan, Y. Zhoua, W. Chen, S. Yang, X. Ren, K. Otsuka, *Mater. Sci. Eng. A* **438-440**, 622 (2006)
- [9] M. Nishida, T. Hara, T. Ohba, K. Yamaguchi, K. Tanaka and K. Yamauchi, *Mater. Trans.* **44 No.12**, 2631 (2003)
- [10] J. Michutta, Ch. Somsen, A. Yawny, A. Dlouhy and G. Eggeler: *Acta Mater.* **54**, 3525 (2006)
- [11] J. Michutta, M. C. Carroll, A. Yawny, Ch. Somsen, K. Neuking and G. Eggeler, *Mater. Sci. Eng. A* **378**, 152 (2004)
- [12] D. Y. Li, L. Q. Chen, *Acta Mater.* **45**, 471 (1997)
- [13] W. Tang, *Metall. Mater. Trans. A*, **28 No.3**, 537 (1997)
- [14] Z. Yang, W. Tirry, D. Schryvers, *Scripta Mater.* **52**, 1129 (2005)
- [15] S. Cao, W. Tirry, W. Van Den Broek and D. Schryvers, *J. Microsc.* **233**, 61 (2009)
- [16] [http://www.sympatec.com/Science/Characterisation/05\\_ParticleShape.html](http://www.sympatec.com/Science/Characterisation/05_ParticleShape.html)
- [17] W.H. Walton, *Nat.* **162**, 329 (1948)
- [18] H. Wadell, *J. Geolo.* **43**, 250 (1935)
- [19] S. Cao, Ch. Somsen, D. Schryvers and G. Eggeler, *Scripta Mater.* (to be published)